Study of Johnson-Cook Model Comprehensiveness at Moderate Strain Rate and Inverse Analysis to Modify the Constitutive Parameters Using Cold Wire Drawing Process

Ashakan Mahmoud Aghdami[1], Behnam Davoodi[2*]
[1]Department of Manufacturing Engineering, Faculty of Mechanical Engineering, University of Tabriz
[2]School of Mechanical Engineering, Iran University of Science and Technology, Tehran, Iran
[*]Email of Corresponding Author: bdavoodi@iust.ac.ir
Received: November 15, 2019; Accepted: February 7, 2020

Abstract
Johnson cook constitutive equation was utilized to model the 10100 copper alloy wires at the cold wire drawing process. Johnson cook parameters were determined using several quasi-static tensile tests at different strain rates. The wire drawing experiments carried out at seven drawing conditions with two areal reductions and four drawing speeds caused the strain rate ranged from 37 to 115 s^{-1}. Wire Drawing forces were measured using a load cell connected to the die. Analytical and finite element with VUHARD subroutine solutions were implemented to calculate the drawing forces using the Johnson cook parameters as well. Results showed that the Johnson cook model with parameters determined from a quasi-static condition was not able to predict the material behavior at the wire drawing process with a moderate strain rate. Inverse analysis using the Newton- Raphson method to minimize the objective function was carried out to modify the Johnson cook parameters. Updated Johnson cook parameters showed much more correlation with experimental results.

Keywords
Johnson- cook, Moderate strain rate, Inverse analysis, Wire drawing

1. Introduction
The wire drawing process consists of reducing the cross-section of wires by forcing them through a series of dies. Most of the studies on the wire drawing process were focused on finding optimum process parameters using finite element methods or by experimental approach [1-4]. He et al. [5] studied the strain rate effect on the flow stress of carbon steel wires without mentioning the material model used. Parnian [6] investigate the strain rate effect on nanostructured and ultra-fine grained microstructure in austenitic stainless steel AISI 304L during the cold wire drawing process. Among the numerous papers published in this field, there is not much work concerning the wire drawing as an intermediate strain rate process [7] as a method to investigate the constitutive equations. Among the empirical or phenomenological based models, Johnson- cook equation [8] is one of the primary constitutive models used widely for metals subjected to a large strain, high strain rate, and high temperature. This equation shows some deviation from experimental results because the original Johnson-Cook model assumes that thermal softening, strain rate hardening, and strain hardening are three independent phenomena and can be isolated from each other [9]. Chen [10] noted the coupling effect of the work hardening and strain rate for 7050-T7451 alloy and also coupled effect of thermal softening and strain rate. In some researches, the strain rate coefficient value was considered as a function of strain and strain rate [11]. The strain rate coefficient was defined as the expression of

strain rate in Ding et al. research [12]. Ding expressed strain rate coefficient as a seven order function of strain rate. Vural [13] proposed a temperature-dependent equation for the strain hardening factor in the JC model. Some researchers adopt the same way of the decoupling of the three terms like the JC model and propose a new reasonably simple phenomenological constitutive model. Shins [14] proposed a model described the copper dynamic behavior in strain rates above 10^4 s^{-1} well enough. Kang [15] modified the strain rate part of the JC model by changing the linear relation of the C parameter to a second-order relation. Since the logarithmic function approaches minus infinity for minimal strain rates, Clausen [16] modified the strain rate hardening part.

Most of the studies on material models were based on results from laboratorial tests such as Hopkinson and Kolsky Bar apparatus [9, 10, 12, 16-21], and fewer investigations were done based on real material forming processes. Optimization and inverse analysis approaches are also implemented on Johnson cook using machining forces and temperature. Chip formation and temperature in the shear zone were the inputs of Ning [22, 23] study to modify the parameters up to 50% from their reference values. A similar approach was used by Agmell [24] to identify the model constants inversely. Inversely calculated JC model parameters from different studies were also compared by Laakso [25]. Friction stir welding was another tool used by Grujicic [26] to adopt the inverse analysis. Faurholdt [27] used in deep drawing process as a large strain method to inversely calculate the JC constants. He used the Levenberg-Marquardt method to minimize the objective function.

In the present work, Johnson cook parameters were determined from quasi-static tensile tests and used to simulate the wire drawing process at seven different reductions and drawing speeds. The difference between drawing forces from experimental and simulation showed that the JC parameters from lower strain rate conditions could not be able to predict material behavior. Hence an inverse analysis was implemented to modify the constants. Simulation with new parameters showed a better correlation with experimental results.

1. Material

Electronic copper C10100 wire with the chemical composition shown in table 1 was used in this research. Chemical analysis was done using the Atomic Emission Spectroscopy. To remove the cold work effects from former drawing processes, wires were annealed at 500 °C for one hour and before using.

Table1. Chemical composition of copper wires

Copper wire	Cu	Pb	Zn	P	O
	99.99%	0.0005%	0.0001%	0.0003%	0.0005%

All specimens were cut in one-meter length with an initial diameter of 3.52 mm. One end of wires was grinded to reduce the diameter to initial pass of wire through the drawing die.

1.1 Quasi-static tensile test

Quasi-static tensile tests were performed on specimens using the SANTAM STM-400 universal testing machine.

Copper wires with a gauge length of 145 mm were fixed on the tensile machine. The test speed was 15 mm/min, and the extensometer was used to accurately read the strain to determine the young modulus and yield stress. True stress- True strain of copper wire is shown in Figure 1.

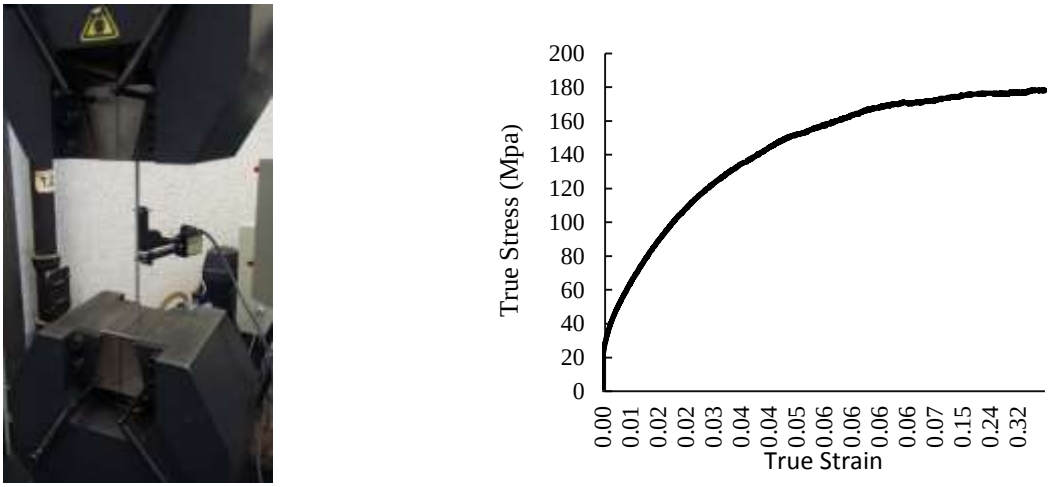

Figure1. True stress- true strain curve of copper 10100 at the quasi-static test

Using the 0.2% offset method, the yield stress for wires calculated as 150 MPa. The reference strain rate acquired from the quasi-static test for copper wires was 1.28×10^{-3} s^{-1}.

2. Johnson-Cook model

This model is appropriate for describing the stress and strain relations of metallic materials under conditions of large deformation, high strain rate, and high temperature. Due to the simple form, it has been widely used soon after it was proposed. The model was expressed as follows:

$$\sigma = (A + B\varepsilon^n)(1 + C \ln \dot{\varepsilon}^*)(1 - (T^*)^m) \quad (1)$$

Where σ is the equivalent stress, ε is the equivalent plastic strain,$\dot{\varepsilon}^* = \dot{\varepsilon}/\dot{\varepsilon}_0$, $\dot{\varepsilon}_0$is the reference strain rate. $T^* = (T - T_r)/(T_m - T_r)$ where, T_r is the room temperature, T_m is the melting point of the material. A is the yield stress at the reference temperature and reference strain rate, B is the coefficient of strain hardening, n is the strain hardening exponent, C and m are the material constants relate to strain rate hardening and thermal softening.

2.1 Determination of work hardening parameters

Considering the plastic part of the stress-strain curve, the work hardening parameters A, B, and n can be determined using the curve fitting method. When $\dot{\varepsilon} = \dot{\varepsilon}_0$ Eq 2 would become:

$$\sigma = (A + B\varepsilon^n) \quad (2)$$

Taking $\dot{\varepsilon}_0 = 1.28 \times 10^{-3}$ s^{-1} as reference strain rate for copper, the A, B, and n were determined using the stress-strain curve from quasi-static tests. Figures 2 shows the work hardening parameters specified through curve fitting for copper wires.

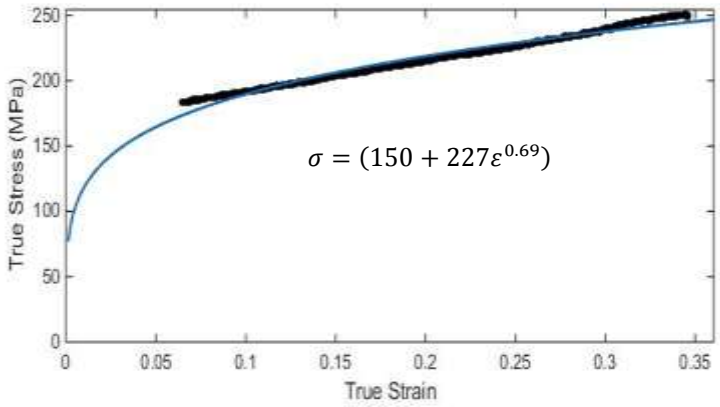

Figure2. Work hardening parameters determined through curve fitting for copper alloy

2.2 Determination of strain rate coefficient

After calculating the work hardening parameters, the JC model can be written as follows:

$$\frac{\sigma}{150 + 227\varepsilon^{0.69}} = 1 + C\ln(\dot{\varepsilon}^*) \quad \text{For Copper} \tag{3}$$

Parameter C is the strain rate sensitivity factor of a material. To determine this parameter, the tensile tests in the previous section were carried out at different strain rates mentioned in Table 2.

Table2. Strain rates carried out for tensile tests

	$\dot{\varepsilon}_1$(s-1)	$\dot{\varepsilon}_2$(s-1)	$\dot{\varepsilon}_3$(s-1)	$\dot{\varepsilon}_4$(s-1)	$\dot{\varepsilon}_5$(s-1)
Copper samples	2.66×10^{-3}	6.38×10^{-3}	3.4×10^{-2}	0.45	1.1

According to the Eq. (5), the parameter C is the slope of the linear relation between $\sigma/(A + B\varepsilon^n)$ and strain rate in different strains. This relation is shown in Figure 3.

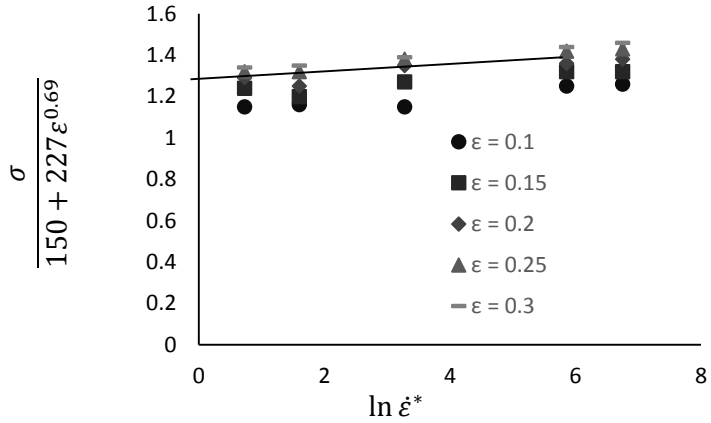

Figure3. $\frac{\sigma}{150+227\varepsilon^{0.69}}$ vs. $\ln \dot{\varepsilon}^*$ for copper wire

By linear curve fitting method, the C constant evaluated as 0.017 for wires.

Temperature rise in wire drawing depends on drawing speed and areal reduction. Haddi et al. [2] studied wire temperature rise in copper wires at different wire drawing conditions. He showed that

there is a linear relationship between temperature ratio (T/T_0) and relative drawing stress(σ_f/σ_0). Experimental results of the present study showed the maximum relative drawing stress of 0.46, which yielded to temperature ratio of 2.3. Taking 25ºC as the reference temperature of wires, the maximum wire temperature at die deformation zone would be 57ºC, which is negligible comparing to the melting point temperature of wires. However, the initial value of 1.09 for constant m of the JC model was taken from the literature [8, 28, 29]. So the JC parameters for copper wires were calculated as follows:

Table3. JC parameters for copper using quasi-static tensile tests

A (MPa)	B (MPa)	n	C	m
150	227	0.69	0.017	1.09

3. Experiments

3.1 Machine

The wire drawing machine used in this article is shown in Figure 4. The machine is driving with a 3Hp electromotor connected to a gearbox. Using an inverter, the rotational speed of the drawing drum was changed to achieve the desire drawing speeds.

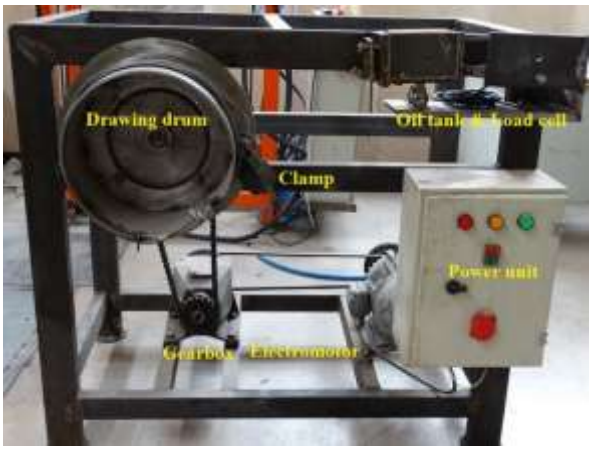

Figure4. Wire drawing machine used

The drawing die was fixed on a lubrication tank, which is connected to the machine body using a bar end joint. There are two rollers under the lubricating tank holding the tank weight and also letting it rotate freely about the bar joint. A load cell was fitted between the lubricating tank and the bar joint so that the drawing force along the wire will be sensed by the load cell. This setup would let the lubricating box and the load cell to align with drawing direction so all the drawing forces in any direction would be sensed by the load cell. Figure 5 shows the die and load cell connection.

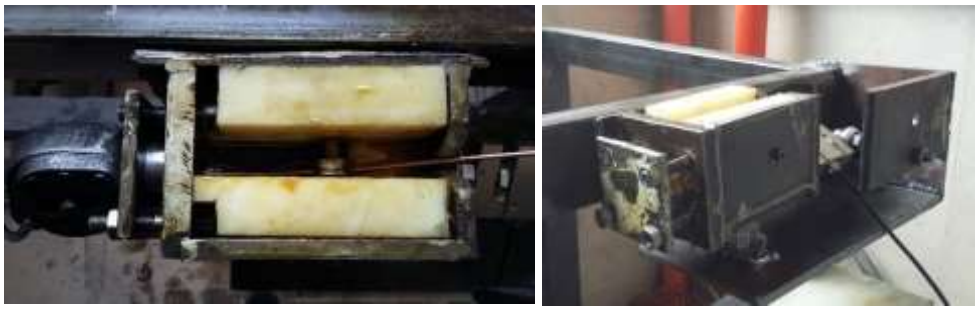

Figure5. Lubricating tank and load cell connection

4.1 Wire drawing tests

The drawing experiments were done at four different drawing speeds and two area reductions. Drawing speeds were set using an inverter connected to the electromotor. Two tungsten carbide dies with the outer diameter of 3.3 mm, and 3.1 mm were used. The engineering strain rate for each test condition was calculated through equation (4).

$$\dot{\varepsilon} = \frac{2ln(D_0/D_1)}{l/v} \tag{4}$$

In this equation, D_0 is the initial wire diameter, D_1 is the die exit diameter, l is the length of the deformation zone, and V is the pulling speed. Testing conditions are shown in table (4). Experiments were done for seven testing conditions shown in table 3, and 7 drawing force curves were obtained.

Table4. Experimental wire drawing conditions for copper wires

	$D_0(mm)$	$D_1(mm)$	r (%)	V (mm/s)	$\dot{\varepsilon}\ (s^{-1})$
Copper wire	3.52	3.3	12	200	37
				400	75
				600	112
				800	150
	3.52	3.1	22	200	38
				400	77
				600	115

Note that drawing speed of 800 mm/s at 22% reduction for copper caused the wires to break.

5. Analytical Solution

The wire drawing process was analyzed through analytical calculation, and the drawing forces obtained for the drawing conditions are mentioned in table 3. Final drawing stress including uniform work, redundant work, and friction work is as follows [30]:

$$\sigma_d = \sigma_a(\ln[1/(1-r)] + (\varphi - 1)\ln[1/(1-r)] + 4\mu\varphi/\Delta) \tag{5}$$

In equation (5), σ_d is the drawing stress of the wire, σ_a is the flow stress of the wire, r is the wire areal reduction. φ is the redundant factor which for typical drawing leads to [30]:

$$\varphi = 0.8 + \Delta/4.4 \tag{6}$$

Approximate value for Δ can calculated as:

$$\Delta = 4\tan\alpha/\ln[1/(1-r)] \tag{7}$$

α is the die semi angle. Combining equation (6) and (7) into the equation (5) and assuming $\tan\alpha \approx \alpha$, the equation (5) would become:

$$\sigma_d = \sigma_a[(3.2/\Delta) + 0.9](\alpha + \mu) \tag{8}$$

Multiplying equation (8) into the exit wire cross area would result in drawing force:

$$F_{draw} = \pi/4\ {D_1}^2\ \sigma_a[(3.2/\Delta) + 0.9](\alpha + \mu) \tag{9}$$

σ_a was considered as the average of the flow stress of entering (σ_{a0}) and exiting (σ_{a1}) wire which means $\sigma_a = (\sigma_{a0} + \sigma_{a1})/2$. As mentioned before, all wires were annealed before entering the die, so σ_{a0} would be equal to wire yield stress, which is 150 MPa. In this case, σ_{a1}would be the JC flow stress. So the σ_a can be rewritten as:

$$\sigma_a = 1/2\left(\sigma_y + (A + B\varepsilon^n)(1 + C\ln\dot{\varepsilon}^*)\right) \tag{10}$$

Substituting the equation (10) into the equation (9) gives the drawing force

$$F_{draw} = \pi/8\ {D_1}^2\left(\sigma_y + (A + B\varepsilon^n)(1 + C\ln\dot{\varepsilon}^*)\right)[(3.2/\Delta) + 0.9](\alpha + \mu) \tag{11}$$

5.1 Coefficient of friction

Avitzur and Evans [31, 32] model is widely used in literature.

$$\frac{\sigma_d}{\sigma_{a0}} = \frac{\left[\frac{\sigma_b}{\sigma_{a0}} + 2f(\alpha)\ln\left(\frac{R_0}{R_1}\right) + \frac{2}{\sqrt{3}}\left(\frac{\alpha}{\sin^2\alpha} - \cot\alpha\right) + 2\mu\left(\cot\alpha\left(1 - \frac{\sigma_b}{\sigma_{a0}} - \ln\left(\frac{R_0}{R_1}\right)\right)\right)\ln\left(\frac{R_0}{R_1}\right) + \frac{P}{R_1}\right]}{\left[1 + 2\mu\frac{P}{R_1}\right]} \tag{12}$$

$$f(\alpha) = \frac{1}{\sin^2\alpha}\left\{1 - (\cos\alpha)\sqrt{1 - \frac{11}{12}\sin^2\alpha} + \frac{1}{\sqrt{11.12}}\ln\frac{1 + \sqrt{\frac{11}{12}}}{\sqrt{\frac{11}{12}}\cos\alpha + \sqrt{1 - \frac{11}{12}\sin^2\alpha}}\right\} \tag{13}$$

In this equation α is the die semi angle, σ_d is drawing stress which is equal to experimental drawing force /exit wire area, σ_0 is the flow stress of initial wire, R_0 is initial wire radius, R_1 is wire radius at die exit, $\frac{\sigma_b}{\sigma_{a0}}$ is relative back stress, P is the die land length. In equation 15, $f(\alpha)$ is 1.00052. According to the avitzur model, the coefficients of friction for experimental drawing conditions in this study are mentioned in table 5.

Table5. Coefficient of friction for drawing conditions

$D_0(mm)$	$D_1(mm)$	V (mm/s)	$\dot{\varepsilon}\ (s^{-1})$	$\sigma_d(MPa)$	μ
3.52	3.3	200	37	86	0.086
		400	75	84.9	0.078
		600	112	83	0.069
		800	150	82.7	0.061
3.52	3.1	200	38	130	0.049
		400	77	129.8	0.046
		600	115	129.7	0.044

As is seen in table 8, by increasing the drawing speed and strain rate, the drawing stress and relative coefficient of friction were reduced.

6. FEM Analysis

The JC parameters acquired from quasi-static tests and coefficient of friction from the previous section were used to simulate the cold copper wire drawing process at different drawing conditions mentioned in table 4, and the drawing forces were generated.

The FEM simulation was done in the ABAQUS commercial code. The wire drawing process was modeled as 2D axisymmetric in explicit dynamic mode. The standard dynamic temperature coupled element was used to solve the problem. The FE model is shown in Figure 6. The JC parameters calculated from quasi-static tests were put as the material model in software. The die was considered as tungsten- carbide material, and the die angle was set to 9 degrees. The ambient temperature was set to 25 °C, and the convection coefficient of air around was set to 15 W/m^{2}K for the boundary condition. The physical and mechanical properties of die and wires are listed in table 6. The die was fixed in both directions on one nod on the die, and drawing direction was from right to left, and the reaction force on fixed nod along pulling direction considered as drawing force. To solve the problem in the plastic region and to introduce the JC constitutive model to the FEM model, a VUHARD subroutine was developed. The JC model and its derivatives respect to strain and strain rate and constitutive parameters were included in the subroutine.

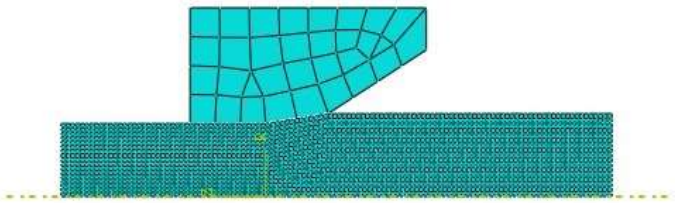

Figure6. FEM model used to simulate the wire drawing process

Table6. Physical and mechanical properties of wire and die material [33, 34]

	Conductivity (W/mK)	Density (kg/m3)	Young modulus (GPa)	Poisson ratio	Expansion coefficient (K-1)	Specific heat (J/kgK)
Copper	391	8900	115	0.3	1.7×10-5	384
Tungsten-Carbide	84	14900	614	0.25	5.2×10-6	210

7. Results

Average drawing forces from experimental tests, analytical solution, and FEM simulation are presented and compared in seven different drawing conditions in table 7 and Figure 7.

Table7. Average drawing force from experimental and simulation results and analytical solution with JC parameters determined from the quasi-static tensile test

$D_0(mm)$	$D_1(mm)$	V (mm/s)	$\dot{\varepsilon}\ (s^{-1})$	$\overline{\mathrm{F}_{exp}}$	F_{ana}	$\overline{\mathrm{F}_{sim}}$	$Error = \frac{\overline{\mathrm{F}_{exp}} - \overline{\mathrm{F}_{sim}}}{\overline{\mathrm{F}_{exp}}} \times 100$
3.52	3.3	200	37	696	630	622	10.6
		400	75	697	613	615	11.7
		600	112	698	592	609	12.7
		800	150	686	573	578	15.7
3.52	3.1	200	38	925	729	740	20
		400	77	951	730	743	21.8
		600	115	956	732	751	21.4

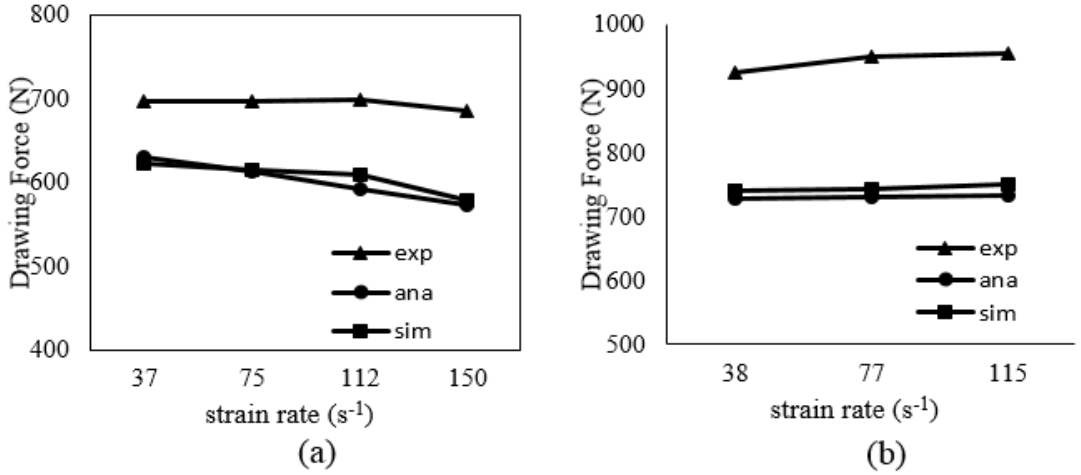

Figure7. Drawing force from experimental, analytical solution and FEM simulation with JC parameters determined from the quasi-static tensile test for (a) output diameter of 3.3 mm and (b) output diameter of 3.1 mm

Simulation and analytical results are considerably close to each other, and it somehow verifies the simulation procedure.

Looking at error amounts between the experimental and simulation results in table 7 shows that in both areal reductions, the error amount gets higher as the strain rate increases. The number of error in lower drawing speeds is smaller compare to higher drawing speeds because in lower drawing speeds, the strain rate in wire drawing is close to quasi-static strain rate condition in which the JC parameters where determined. By extending the strain rates to higher values, the error increases. This is one of the primary deficiencies of the JC model, which confines it to specific strain rates, and parameters have to be updated as the deformation conditions change.

In the wire drawing process, two phenomena have the opposite effect on drawing force. As the drawing speed and the strain rate elevates, the flow stress of wires increases due to the JC constitutive relation. On the other hand, friction decreases as the drawing speed increases. At

drawing with 3.3 mm die, the lubrication condition changed from almost boundary type lubrication (μ = 0.086) to near thick film lubrication (μ = 0.061) [30], So the strain rate and the friction are in close competition to control the drawing force and resulted in almost constant drawing force with drawing speed changes. But at drawing with 3.1 mm die, lubrication performance was better, and the coefficient of friction was at its minimum value of μ = 0.04. So by increasing the drawing speed and the strain rate, the friction force did not change, but the flow stress increased due to the JC equation and caused the drawing force to grow as well.

8. Inverse analysis

To update the JC parameters, an inverse method was used [35]. An objective function in a least square sense was defined as equation (14):

$$E(p_k) = \frac{1}{N}\sum_{i=1}^{N}\left(\frac{F_{exp} - F_{ana}(p_k)}{F_{exp}}\right)^2 \tag{14}$$

Where N is the number of sampling points in drawing force vs. time curve, p_k is the number of JC equation parameters. When the $E(p_k)$ is minimized, the JC parameters were determined. The F_{ana} was obtained from F_{sim}. For given JC parameters p_k, the objective function will be minimum at:

$$\frac{\partial E(p_k)}{\partial p_k} = 0 \qquad k = 1,2,\dots,q \tag{15}$$

q is the number of rheological parameters of the JC model.

The first prentices of the JC model (eq.1) is related to the plastic region of the material. This part can be determined through the quasi-static test, which was presented in section 2.1. So the parameters A, B, and n were remained unchanged during the inverse process, and only parameters C and m in eq.1 were changed during the inverse analysis. So the $k = 2$ and eq (15) would become:

$$\frac{\partial E(C)}{\partial C}, \frac{\partial E(m)}{\partial m} = 0 \tag{16}$$

Using the Newton-Raphson iterative algorithm to solve the eq (16):

$$\frac{\partial^2 E(p_k)}{\partial {p_k}^2}\Delta p_{k\,j} = -\frac{\partial E(p_k)}{\partial p_k} \qquad j = 1,2,\dots,q \tag{17}$$

q is the number of iterative to get the final C and m values. Taking the derivatives of the objective function with respect to c:

$$\frac{\partial E(p_k)}{\partial p_k} = -\frac{2}{N}\sum_{i=1}^{N}\left\{\frac{(F_{exp} - F_{ana})}{{F_{exp}}^2}\frac{\partial F_{ana}}{\partial p_k}\right\} \tag{18}$$

$$\frac{\partial^2 E(p_k)}{\partial {p_k}^2} = -\frac{2}{N}\sum_{i=1}^{N}\left\{\frac{-1}{{F_{exp}}^2}\left(\frac{\partial F_{ana}}{\partial p_k}\right)^2 + \frac{(F_{exp} - F_{ana})}{{F_{exp}}^2}\frac{\partial^2 F_{ana}}{\partial {p_k}^2}\right\} \quad (19)$$

Where $\frac{\partial F_{ana}}{\partial p_k}$ and $\frac{\partial^2 F_{ana}}{\partial {p_k}^2}$ are the first and the second derivatives of parameters C and m. Taking the first and second derivative of drawing force with respect to C and m:

$$\frac{\partial F_{ana}}{\partial C} = \pi/8\ {D_1}^2\ [(3.2/\Delta) + 0.9](\alpha + \mu)(A + B\varepsilon^n)(1 - (T^*)^m)\ln \dot{\varepsilon}^* \quad (20)$$

$$\frac{\partial F_{ana}}{\partial m} = -\pi/8\ {D_1}^2\ [(3.2/\Delta) + 0.9](\alpha + \mu)(A + B\varepsilon^n)(1 + C\ln \dot{\varepsilon}^*)\ln T^*(T^*)^m \quad (21)$$

$$\frac{\partial^2 F_{ana}}{\partial C^2} = 0 \quad (22)$$

$$\frac{\partial^2 F_{ana}}{\partial C \partial m} = \frac{\partial^2 F_{ana}}{\partial m \partial C} = -\pi/8\ {D_1}^2\ [(3.2/\Delta) + 0.9](\alpha + \mu)(A + B\varepsilon^n)\ln T^* \ln \dot{\varepsilon}^*\ (T^*)^m \quad (23)$$

$$\frac{\partial^2 F_{ana}}{\partial m^2} = -\pi/8\ {D_1}^2\ [(3.2/\Delta) + 0.9](\alpha + \mu)(A + B\varepsilon^n)(1 + C\ln \dot{\varepsilon}^*)\ln {T^*}^2\ (T^*)^m \quad (24)$$

By substituting equations 20- 24 into the equations 18 and 19, and supposing an initial value of parameter C and m of the JC model as $C = 0.017, m = 1.09$ form quasi-static tests and literature, new values for C and m were calculated. Simulation with the new value of C and m was carried out, and new drawing forces were generated. This process continues until the equation 15 was close enough to its root value, and at this point, the C and m were identified. The overall procedure is shown in Figure 8:

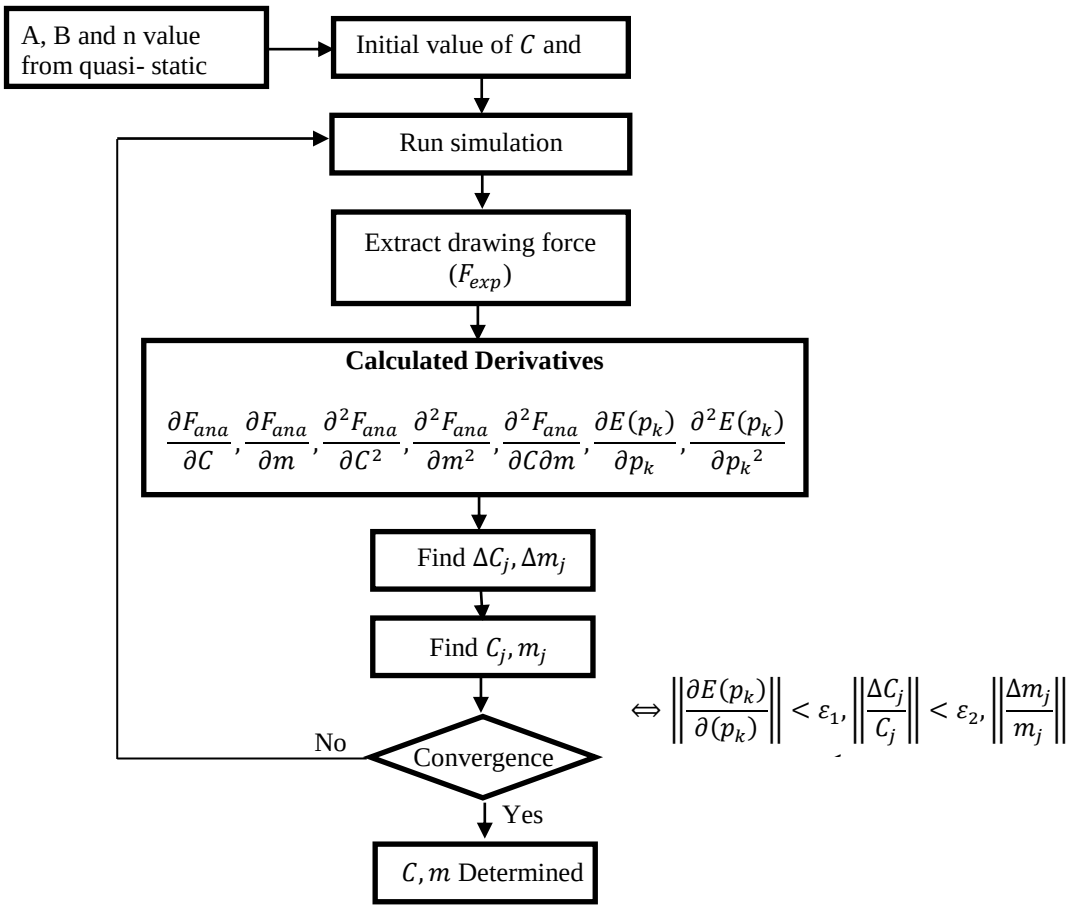

Figure8. Flow chart of the inverse process to determine the C and m parameters of the JC model

The progressive C and m values are shown in table 8. The convergence criteria ε_1, ε_2, and ε_3 were set to 0.02, 0.02, and 0.03 respectively.

Table8. C values at each inverse analysis step

Iteration	initial	#1	#2	#3	#4	#5	#6
C	0.017	0.0395	0.0288	0.0337	0.0314	0.0325	0.0320
m	1.09	1.05	1.09	1.13	1.10	1.07	1.04

After six iterations, the C and m values met the convergence criteria, and the inverse solution code stopped. Determining the new values of C and m, the updated JC parameters for copper wires are as shown in table 9:

Table9. updated JC parameters for copper wires after running the inverse analysis

A (MPa)	B (MPa)	n	C	m
150	227	0.69	0.032	1.04

Simulation drawing results with the updated JC parameters from inverse analysis along with error content in table 10 and Figure 9 show that the error content reduced to utmost 4%.

Table10. Average drawing force from experimental and simulation results and analytical solution with updated C and m parameters using inverse analysis

$D_0(mm)$	$D_1(mm)$	V (mm/s)	$\dot{\varepsilon}\ (s^{-1})$	$\overline{F_{exp}}$	$\overline{F_{sim}}$	$Error = \frac{\overline{F_{exp}} - \overline{F_{sim}}}{\overline{F_{exp}}} \times 100$
3.52	3.3	200	37	696	676	2.84
		400	75	697	675	2.89
		600	112	698	677	2.92
		800	150	686	672	2.01
3.52	3.1	200	38	925	883	4.51
		400	77	951	908	4.52
		600	115	956	917	4.0

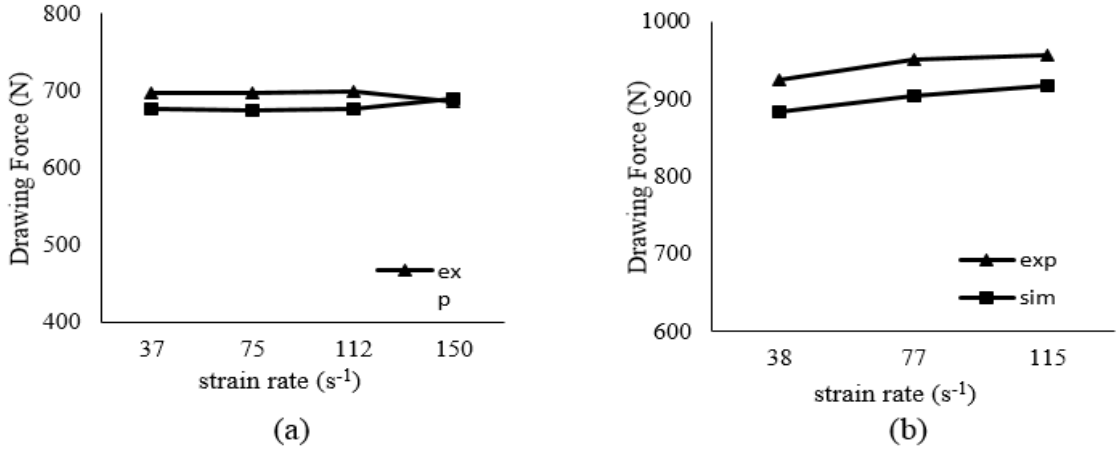

Figure9. Drawing forces from experimental and simulation results with updated C parameter using inverse analysis for (a) output diameter of 3.3 mm and (b) output diameter of 3.1 mm

9. Conclusion

In the present work, the Johnson- cook parameters A, B, n, and C for 10100 copper alloy were determined using several quasi-static tensile tests, and the parameter m from literature. These parameters were used to FEM simulation and analytical solution of the wire drawing process. Comparison of wire drawing forces from experimental tests to simulation and analytical results showed that the JC parameters obtained from low strain rate did not accurately predict the material behavior at the wire drawing process with moderate strain rates. The inverse analysis was implemented using the Newton- Raphson method to minimize the objective function. The C and m constant of the JC model were modified after six consecutive iterations until their values matched the convergence criteria. Simulation results with updated JC parameters showed a very good correlation with experiments, and the error content reduced to 2 to 4% in seven drawing conditions.

10. References

[1] Vega, G., Haddi, A. and Imad, A. 2009. Investigation of process parameters effect on the copper-wire drawing. Materials & Design. 30(8):3308-3312.

[2] Haddi, A., Imad, A. and Vega, G. 2011. Analysis of temperature and speed effects on the drawing stress for improving the wire drawing process. Materials & Design. 32(8-9):4310-4315.

[3] Luis, C., Leon, J. and Luri, R. 2005. Comparison between finite element method and analytical methods for studying wire drawing processes. Journal of materials processing technology. 164:1218-1225.
[4] Celentano, D.J., Palacios, M.A. Rojas, E.L. M.A., Cruchaga, A.A. Artigas, and Monsalve, A.E. 2009. Simulation and experimental validation of multiple-step wire drawing processes. Finite Elements in Analysis and Design. 45(3):163-180.
[5] He, S., Van Houtte, P., Van Bael, A., Mei, Sarban, F., Boesman, A. P., Gálvez, F. and Atienza, J. 2002. Strain rate effect in high-speed wire drawing process. Modelling and Simulation in Materials Science and Engineering. 10(3): 267-270.
[6] Parnian, P. and Parsa, M. 2015. The Effect of Strain Rate on Ultra-Fine Grained Structure of Cold Drawn 304L Stainless Steel Wires. Procedia Materials Science. 11: p. 24-31.
[7] Committee, A.I.H., ASM handbook: mechanical testing and evaluation. 2000. ASM International.
[8] Johnson, G.R. and Cook, W.H. 1983. A constitutive model and data for metals subjected to large strain, high strain rates and high temperatures. Proceedings of the 7th International Symposium on Ballistics.
[9] Lin, Y., Chen, X.-M. and Liu, G. 2010. A modified Johnson–Cook model for tensile behaviors of typical high-strength alloy steel. Materials Science and Engineering: A. 527(26): 6980-6986.
[10] Chen, G., Ren, C., Ke, Z., Li, J. and Yang, X. 2016. Modeling of flow behavior for 7050-T7451 aluminum alloy considering microstructural evolution over a wide range of strain rates. Mechanics of Materials. 95:146-157.
[11] Tan, J.Q., Zhan, M., Liu, S., Huang, Guo, T. J. and Yang, H. 2015. A modified Johnson–Cook model for tensile flow behaviors of 7050-T7451 aluminum alloy at high strain rates. Materials Science and Engineering: A. 631:214-219.
[12] Zhang, D.-N., Shangguan, Q.-Q., Xie, C.-J. and Liu, F. 2015. A modified Johnson–Cook model of dynamic tensile behaviors for 7075-T6 aluminum alloy. Journal of Alloys and Compounds. 619:186-194.
[13] Vural, M. and Caro, J. 2009. Experimental analysis and constitutive modeling for the newly developed 2139-T8 alloy. Materials Science and Engineering: A. 520(1-2):56-65.
[14] Shin, H. and Kim, J.-B. 2010. A phenomenological constitutive equation to describe various flow stress behaviors of materials in wide strain rate and temperature regimes. Journal of Engineering Materials and Technology. 132(2):021009.
[15] Kang, W., Cho, S., Huh, H. and Chung, D. 1999. Modified Johnson-Cook model for vehicle body crashworthiness simulation. International Journal of Vehicle Design. 21(4):424-435.
[16] Clausen, A.H., Børvik, T., Hopperstad, O.S. and Benallal, A. 2004. Flow and fracture characteristics of aluminium alloy AA5083–H116 as function of strain rate, temperature and triaxiality. Materials Science and Engineering: A. 364(1-2):260-272.
[17] Li, H.-Y., Li, Y.-H., Wang, X.-F., Liu, J.-J. and Wu, Y. 2013. A comparative study on modified Johnson Cook, modified Zerilli–Armstrong and Arrhenius-type constitutive models to predict the hot deformation behavior in 28CrMnMoV steel. Materials & Design. 49:493-501.

[18] Majzoobi, G., Freshteh-Saniee, F., Khosroshahi, S.F.Z. and Mohammadloo, H.B. 2010. Determination of materials parameters under dynamic loading. Part I: Experiments and simulations. Computational Materials Science. 49(2):192-200.
[19] Iwamoto, T. and Yokoyama, T. 2012. Effects of radial inertia and end friction in specimen geometry in split Hopkinson pressure bar tests: a computational study. Mechanics of Materials. 51:97-109.
[20] Bhaduri, A., Mechanical Properties and Working of Metals and Alloys. 2018: Springer.
[21] Majzoobi, G.-H., Hosseinkhani, A.R., Lahmi, S., Pipelzadeh, M.K. and Hardy, S.J. 2014. Determination of the constants of material models at high strain rates and elevated temperatures using shot impact test. The Journal of Strain Analysis for Engineering Design. 49(5):342-351.
[22] Ning, J. and Liang, S.Y. 2018. Model-driven determination of Johnson-Cook material constants using temperature and force measurements. The International Journal of Advanced Manufacturing Technology. 97(1-4):1053-1060.
[23] Ning, J., Nguyen,V., Huang, Y., Hartwig, K.T. and Liang, S.Y. 2018. Inverse determination of Johnson–Cook model constants of ultra-fine-grained titanium based on chip formation model and iterative gradient search. The international journal of advanced manufacturing technology. 99(5-8): 1131-1140.
[24] Agmell, M., Ahadi, A. and Ståhl, J.-E. 2014. Identification of plasticity constants from orthogonal cutting and inverse analysis. Mechanics of Materials. 77:43-51.
[25] Laakso, S.V. and Niemi, E. 2017. Using FEM simulations of cutting for evaluating the performance of different johnson cook parameter sets acquired with inverse methods. Robotics and Computer-Integrated Manufacturing. 47: 95-101.
[26] Grujicic, M., Pandurangan, B., Yen, C.-F. and Cheeseman, B. 2012. Modifications in the AA5083 Johnson-Cook material model for use in friction stir welding computational analyses. Journal of Materials Engineering and Performance. 21(11):2207-2217.
[27] Faurholdt, T.G. 2000. Inverse modelling of constitutive parameters for elastoplastic problems. The Journal of Strain Analysis for Engineering Design. 35(6):471-478.
[28] Frutschy, K. and Clifton, R. 1998. High-temperature pressure-shear plate impact experiments on OFHC copper. Journal of the Mechanics and Physics of Solids. 46(10):1723-1744.
[29] Assadi, H., Gärtner, F., Stoltenhoff, T. and Kreye, H. 2003. Bonding mechanism in cold gas spraying. Acta Materialia. 51(15):4379-4394.
[30] Wright, R.N. 2011. Wire Drawing Technology: Process Engineering and Metallurgy. USA: Elsevier Inc.
[31] Evans, W. and Avitzur, B. 1968. Measurement of friction in drawing, extrusion, and rolling. Journal of Lubrication Technology. 90(1): 72-80.
[32] Avitzur, B. 1963. Analysis of wire drawing and extrusion through conical dies of small cone angle. Journal of Engineering for Industry. 85(1): 89-95.
[33] Richardson, H.W. 1997. Handbook of copper compounds and applications. CRC Press.
[34] Kurlov, A. and Gusev, A. 2013. Tungsten Carbides: Structure, Properties and Application in Hardmetals. Springer, Cham-Heidelberg-NY.

[35] Cho, H. 2007. Development of Advanced Techniques for Identification of Flow Stress and Friction Parameters for Metal Forming Analysis, Doctor of Philosophy, Ohio State University, Industrial and Systems Engineering.